Journal of Petroleum Exploration and Production Technology (2018) 8:1099–1112
https://doi.org/10.1007/s13202-018-0473-0

ORIGINAL PAPER - EXPLORATION GEOLOGY

Microscopic pore structure of Chang 6_3 reservoir in Huaqing oilfield, Ordos Basin, China and its effect on water flooding characteristics

Pan Li[1,2] · Wei Sun[1,2] · Jian Yan[3] · Rui Huang[4] · Hexin Huang[1,2]

Received: 12 January 2018 / Accepted: 10 May 2018 / Published online: 13 July 2018

Abstract

Chang 6_3 reservoir in Huaqing oilfield, Ordos Basin, China is featured by strong pore structure heterogeneity, which leads to prominent Jamin effect in the water flooding, difficult development process, low productivity, and massive residual oil. Accordingly, this study aims to explore the microscopic pore structure of Chang 6_3 reservoir and investigate its influence on the water flooding efficiency, based on a series of comprehensive analyses, including physical property analysis, casting thin section observation, scanning electron microscopy measurement, high-pressure mercury injection, constant rate mercury injection, and microscopic real sandstone water flooding model. It is demonstrated that gray and gray-brown feldspathic sandstone are the main reservoir lithology in the study area, with dominant pore types of residual intergranular pores and feldspar dissolution pores. Pore throat radius is unevenly distributed, and small and micro pores take the majority. Based on the comparison of capillary pressure curve characteristics and comprehensive analysis of corresponding parameters, the pore structure of the Chang 6_3 reservoir is divided into four types, namely types I–IV. They have different reservoir spaces, and their reservoir and seepage capacities decrease in the order of types I–IV pore structures. Moreover, displacement patterns in them are also different, with the finger-like-reticular displacement as the primary. In addition, pore throat radius and distribution play a critical role in the water flooding. It is also demonstrated that the water flooding efficiency increases with permeability and porosity, pore structure quality, and pore throat distribution evenness.

Keywords Microscopic pore structure · Water flooding experiment · Huaqing oilfield · Physical properties · Pore structure type

Introduction

Abundant in oil, Yanchang Formation in the east of Ordos Basin has been one of the most important targets in the ultra-low permeability and tight sandstone reservoir development. Specifically, the third sub-member of the sixth member of Yanchang Formation (Chang 6_3) is the most representative (Gao et al. 2013; Huang et al. 2016; Ren et al. 2015a; Shi et al. 2016) (Fig. 1). Previous studies demonstrate the strong microscopic heterogeneity of Chang 6_3 reservoir sand body in Huaqing oilfield, which leads to prominent Jamin effect in the late water flooding, difficult development process, low productivity, and massive residual oil, thereby significantly restricting the effective development of Huaqing oilfield (Qu et al. 2016; Ren et al. 2015; Zhang et al. 2015a, b). The water flooding efficiency is found to be closely related to the microscopic pore structure of the reservoir, which has not been sufficiently addressed in the previous studies (Zhao et al. 2012). Moreover, fluid flow and migration in the reservoir pore space can be intuitively observed in the water flooding experiment in the microscopic real sandstone model under the microscope, which can help analyze the rule of water flooding and the controlling factors of water flooding efficiency in conditions with different types of microscopic pore structures (Bai et al. 2016; Halim et al. 2015). With regard to the microscopic real sandstone model, it is a patented technology of the National Key Laboratory of

✉ Pan Li
122078558@qq.com

[1] State Key Laboratory of Continental Dynamics of Ministry of Geology, Northwest University, Xi'an 710069, China

[2] Department of Geology, Northwest University, Xi'an 710069, China

[3] College of Petroleum Engineering, Xi'an Shiyou University, Xi'an 710065, China

[4] CNPC, Richfit Information Technology Co. Ltd, Beijing 100000, China

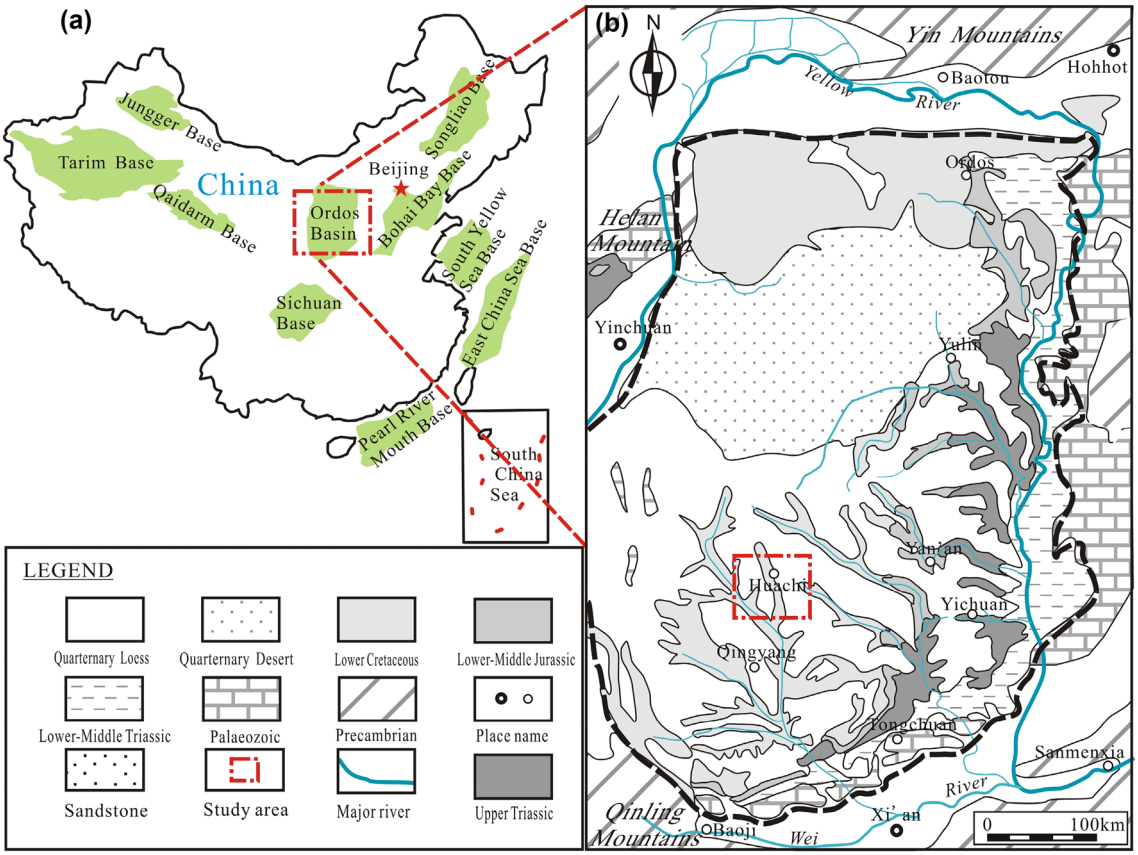

Fig. 1 Geographic location of Huaqing oilfield **b** in the Ordos Basin (**a**)

Continental Dynamics of Northwest University, China. Its delicate microscopic model production technology enables the reservoir rock to retain not only the initial pore structures but also the rock surface physical properties and interstitials, thereby greatly increasing the model credibility and application range (Zhao et al. 2017). The coupling of microscopic real sandstone model and full information scan video can realistically and intuitively reshow the fluid motion and residual oil distribution in the oil–water two-phase displacement process, so that the displacement characteristics of the fluids in the rock pore space can be directly observed (Cao et al. 2016; Wang et al. 2008; Yadali and Kharrat 2009; Yan et al. 2017).

In recent years, lots of works have been done on the microscopic displacement characteristics of oil and water in reservoirs, which achieve much progress both technically and theoretically. Specifically, displacement experiments in the conventional cores are upgraded to those in the current microscopic real sandstone model that enables observation of oil and water movements under the microscope, which makes it possible to implement real-time observation and quantitative description analysis (Clarkson et al. 2012; Guo et al. 2007; Jia 2017; Xia et al. 2013). However, there are relatively few studies on the microscopic displacement characteristics of oil and water in ultra-low permeability reservoirs, which needs to be further improved and supplemented. It is demonstrated that the oil–water two-phase microscopic displacement characteristics of ultra-low permeability sandstone reservoirs are obviously different from those conventional reservoirs. For example, the wettability of ultra-low permeability reservoirs has a certain impact on the residual oil distribution and water flooding efficiency; especially, the ultimate oil displacement efficiency is strongly influenced by the microscopic heterogeneity of the pore structure; Jamin effect has a prominent effect on the water flooding efficiency after contact with water, in the form of increased water injection resistance and increased injection pressure (Ge et al. 2015; Kamath et al. 1993; Liu et al. 2002; Qin et al. 2010; Rabiei et al. 2013; Zhang et al. 2012a). With the increase of the injection pressure, the injected water forms a new percolation channel, and the previously formed channel is "locked up". The oil droplets remaining at the pore throat are only deformed but are difficult to migrate due to the additional capillary resistance. (Dastgheib et al. 2008; Song et al. 2015) In this case, fluid seepage only occurs in the partially interconnected macro pores under the influence of the pore structure heterogeneity. Consequently, oilfield development methods that are suitable

for medium and high-permeability reservoirs have encountered difficulties in ultra-low permeability reservoirs (Kaster et al. 2012; Li et al. 2007; Yadali and Kharrat 2010). Accordingly, much attention has been paid to analyzing the characteristics of microscopic oil–water displacement as well as identifying the movement and distribution rules of oil and water. Specifically, these works regard the microscopic pore structure of reservoirs to be a critical factor in impacting the characteristics of microscopic oil–water displacement. Relevant works are mainly conducted in the microscopic model displacement experiments (Wang and Gu 2011; Yang et al. 2013; Zheng and Liu 2015; Zhou et al. 2016).

To more scientifically apply the microscopic real sandstone water flooding model to improve the reservoir evaluation, this study comprehensively employs physical property analysis, casting thin section observation, scanning electron microscopy analysis, and high-pressure mercury injection test on the Chang 6_3 reservoir in Huaqing oilfield. Correspondingly, microscopic pore structure characteristics, physical properties, water flooding characteristics, and average pore throat radius are compared and analyzed to characterize the microscopic pore structure of Chang 6_3 reservoir and explore its influence on the water flooding efficiency. Results of this study are expected to provide certain theoretical guidance on the design of proper development scheme, the optimization of injection parameters, and the adjustment of operation plan.

Geological setting and experimental description

Geological background and samples

Spanning Shaanxi, Gansu, Ningxia, Inner Mongolia and Shanxi Provinces, Ordos Basin is the second largest sedimentary basin in China with an area of about 250,000 km^2. It is surrounded by mountains, and hosts the branches of Yellow River and Weihe River. The Ordos Basin is roughly bounded by the Great Wall in the north, with the Ordos Plateau in the north and the Loess Plateau in the south. Specifically, the Ordos Plateau, with an elevation of 1200–1500 m, is home to widely distributed eolian sand dunes and deserts, and in the locally low areas there are a few saline–alkali lakes, all of which are possibly due to the dry climate and insufficient water resources; the Loess Plateau in the south is of an elevation of 800–1600 m (Dong et al. 2006).

Geographically in the Huachi and Qingyang Counties of Gansu Province, Huaqing oilfield is tectonically located in the western part of the Shaanbei Slope Belt, where Triassic Yanchang Formation and Jurassic Yan'an Formation are the main two oil-bearing successions with dominant lacustrine delta front and deep water gravity flow deposits. According to the characteristics of lithology, electricity and sedimentary cycles, the Triassic Yanchang Formation of Huaqing oilfield is divided into ten oil reservoir sets from bottom to top. Among them, the Chang 6_3 reservoir is the target of this study. During the deposition of Yanchang Formation in the Late Triassic, there are mainly two provenances in the basin, respectively, from the northeast and southwest. Influenced by the steep topography in the southwest and gentle topography in the northeast, rivers–alluvial plains–meandering river deltas are the main sedimentary facies in the northeast, while alluvial fan and braided river delta are dominant in the southwest. Specifically impacted by the northeastern provenance during the Late Triassic, multiple assemblages of source, reservoir and cap rocks are formed, constituting the basic geological conditions for hydrocarbon accumulation (Suthar et al. 2008; Wardlaw 1982).

The sandstones of Chang 6_3 reservoir in Huaqing Area are mainly fine-grained and very fine-grained, with main lithology of gray-black, gray, gray-white feldspathic sandstone and lithic feldspar sandstone (Kate and Gokhale 2006; Papadimitriou et al. 2007). Pore combination types mainly include intergranular pore–dissolution pore and dissolved pore–intergranular pore. The interstitials are mainly matrix and cements, whereas cements primarily include hydromica, chlorite, ferrocalcite, ankerite, calcite, siliceous matter, and a small amount of argillo ferruginous substance. The rocks are featured by moderate to good sorting, poor roundness with dominant sub-angular shapes and a few angular shapes, primary pore cementation (followed by overgrowth and thin film cementation), and presence of illite, chlorite and illite/smectite mixed layers.

A total of 11 core samples are implemented with microscopic real sandstone water flooding experiments, which are combined with analyses of conventional physical properties (189 samples), casting thin sections (98 samples), electron microscopy scanning (62 samples), high-pressure mercury injection (31 samples) and constant rate mercury intrusion (15 samples), so as to analyze the microscopic water flooding characteristics of different pore structure types. The clay mineral filling content and physical property data can be obtained through analyses of casting thin sections and image grain sizes; pore structures are classified into four types according to the high-pressure mercury injection experiments; pore radius and throat radius, pore throat radius ratio, sorting coefficient, and movable fluid saturation can be acquired by constant rate mercury intrusion tests; microscopic real sandstone water flooding experiment can be used to explore the oil and water displacement characteristics in different microscopic pore structures, which can reflect the seepage ability of the reservoir (Table 1).

Table 1 Parameters of microscopic real sandstone water flooding experiments on the Chang 6_3 reservoir with different pore structure types in Huaqing oilfield

Sample ID	Well ID	Depth/m	Liquid permeability/$\times10^{-3}\mu m^2$	Porosity/%	Surface porosity/%	Intergranular pore/%	Feldspar dissolution pore/%	Pore type
1	W38	2043.35	0.6323	13.43	4.8	3.7	0.9	Dissolution pore–intergranular pore
2	L87	2195.45	0.2884	8.7	0.7	0.2	0.3	Intergranular pore–dissolution pore
3	B461	1985.71	0.3386	9.37	0.9	0.1	0.8	Intergranular pore–dissolution pore
4	S156	2071.45	0.1512	9.03	1	0.1	0.2	Dissolution pore
5	B168	2084.55	0.1622	8.93	0.7	0.2	0.5	Dissolution pore
6	B259	2191	0.1811	10.53	1.5	0.9	1.1	Dissolution pore
7	W61	2017.95	0.0033	6.79	0.6	1.8	0.5	Dissolution pore
8	X245	1976.8	0.0511	6.18	0.5	0.1	0.2	Dissolution pore
9	Y414	1999.45	0.212	10.41	2	14	0.3	Dissolution pore
10	B181	2073.2	0.1028	7.82	0.5	0.1	0.4	Dissolution pore
11	W71	1948.57	0.311	5.22	0.4	0.2	0.5	Dissolution pore

Experimental methods and procedures

Experimental principle of microscopic real sandstone water flooding model

The microscopic real sandstone water flooding experiment is an application of a visualized microscopic reservoir model with the aid of microscope magnification, video recording, image analysis, and experimental metrology technique, which aims to achieve quantitative description of microscopic reservoir fluid seepage and thus reveal the microscopic seepage flow characteristics and microscopic residual oil distribution patterns. The key lies in the establishment of microscopic reservoir models and experimental testing techniques (Ma et al. 2016; Zhang et al. 2012b, 2016). In this study, the real reservoir core is used as the research model. The self-made simulation oil and water are, respectively, used to simulate the crude oil and water in the formation, with their viscosity proportion equal to the actual one. The self-made simulated oil and water are immiscible and can exist simultaneously in the reservoir pore and throat. The simulated water phase is used to displace the simulated oil phase until the content of the simulated oil phase in the core is approximately the same as the actual oil saturation. When the formation temperature and original distribution is reached, the core is consolidated (Lappin-Scott et al. 1988; Zanganeh et al. 2012; Zhang et al. 2012a, 2015b).

Simulation oil and water can be distinguished by their distinctly stained colors. Thin section preparation and microscopic image processing techniques are used to analyze the microscopic distribution of oil and water. Such method fails to reflect the dynamic characteristics of fluid seepage, but does succeed to make the oil and water distribution in the pore throat after displacement closer to the actual condition. Therefore, more direct insights can be gained concerning the oil and water distribution characteristics and patterns.

Microscopic water flooding experimental process

1. Model preparation

In this study, a total of 11 core models are prepared, with the size of 2.5 cm × 2.5 cm × 0.5 cm and the pressure resistance of 0.15 MPa. In the condition that the pore structures are maintained, the 11 core models are first removed of oil and dried, then sliced and polished, after which the polished thin sections are bonded two glass sheets. Then, after consolidation of adhesive, the microscopic core model is prepared. In this study, the simulation water is actually the formation water mixed with methyl blue staining reagent, while the simulation oil is the mixture of crude oil and kerosene formulated with different viscosities and added with oil-soluble red staining reagent.

2. Experimental device

The microscopic model experiment system adopts the seepage flow experimental equipment developed by the Department of Geology of Northwest University, China, including vacuum pumping equipment, pressurized equipment, image acquisition equipment, and microscopic observation equipment. The nitrogen gas cylinder is employed for pressurization, and the digital pressure gauge is used for pressure measurement. The image acquisition system

equipped with a camera can convey the acquired video signal to computer for later observation. The microscopic observation equipment is mainly an Olympus stereo microscope equipped with camera and video functions.

3. Experimental procedure

(a) The model is prepared and dried at a temperature of 40 °C; (b) the gas permeability is measured; (c) the model is vacuumized and then saturated with water; (d) the liquid permeability is measured; (e) the model is saturated with oil; (f) oil is displaced by water flooding (Table 1; Fig. 2).

Characterization of pore throat structure by high-pressure mercury injection and constant rate mercury injection

In the high-pressure mercury injection experiment, mercury is injected into the rock sample through pressurization of it. The pore throat size and its distribution are calculated based on the magnitude of the pressure and the amount of mercury injection, which can be combined with the capillary pressure curve form to quantitatively evaluate the microscopic pore structure characteristics. Through the comprehensive analysis and comparison of the high-pressure mercury injection experimental data and capillary pressure curve characteristics of 31 samples in the study area, the pore structure of Chang 6_3 reservoir in Huaqing oilfield can be divided into four types, namely type I, type II, type III, and type IV (see Table 2; Fig. 5).

Constant rate mercury injection technique is an important means to characterize the microscopic pore throat structure of reservoirs, and it can accurately separate pores and throats. The constant rate mercury injection experiment is implemented using the ASPE-730 constant rate mercury injection device produced by Coretest Systems Company. A total of 15 standard cores with the diameter of 2.5 cm are drilled in the full-diameter core, and then dried at 50 °C after polishing. When the core sample is soaked in the mercury solution after vacuumization, mercury is pumped into the core at a constant, extremely low rate (0.00005 ml/min). The pressure repeatedly drops and rises as the mercury enters the process, and the experiment is stopped when the pressure reaches 900 psi, i.e., 6.2055 MPa. At this time, the radius of the corresponding throat is about 0.12 μm. Real-time

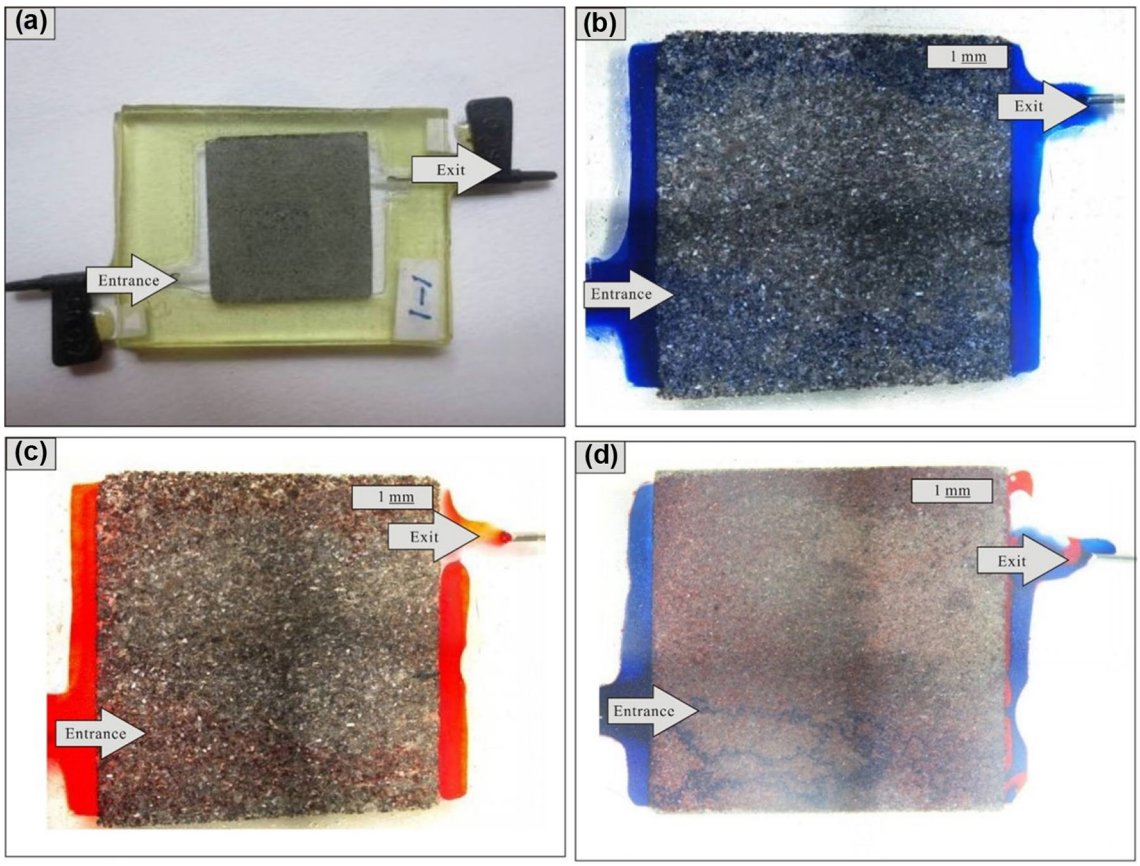

Fig. 2 The microscopic real sandstone model of Chang 6_3 reservoir in Huaqing oilfield. **a** Microscopic sandstone model. **b** Water-saturated model. **c** Oil-saturated model. **d** Water flooding model

Table 2 Conventional mercury injection parameters concerning pore structure of Chang 6_3 reservoir in the study area

Parameters	I		II		III		IV	
	Mean	Range	Mean	Range	Mean	Range	Mean	Range
Permeability/$\times10^{-3}\mu m^2$	0.43	0.31–0.63	0.23	0.18–0.29	0.14	0.09–0.21	0.03	0.003–0.05
Porosity/%	11.66	6.7–20.7	9.03	8.7–9.8	7.85	6.79–8.93	5.7	5.2–6.2
Mean	11.19	10.27–12.08	11.95	10.31–12.72	12.43	11.44–12.99	12.69	11.85–13.27
Sorting coefficient	1.9	1.32–2.53	1.63	0.8–2.46	1.34	0.79–2.61	1.07	0.52–1.99
Variable coefficient	0.18	0.15–0.25	0.14	0.1–0.24	0.15	0.09–1.09	0.11	0.07–0.94
Displacement pressure/Mpa	0.8	0.46–1.07	1.44	0.72–2.31	2.3	1.49–3.22	2.84	1.91–3.79
Maximum pore throat radius/μm	0.98	0.69–1.61	0.32	0.55–1.01	0.33	0.23–0.49	0.29	0.14–0.37
Median pressure/Mpa	3.27	1.75–6.33	4.93	3.14–8.75	8.26	4.11–15.99	10.37	5.98–19.27
Median radius/μm	0.27	0.12–0.42	0.16	0.08–0.23	0.1	0.05–0.18	0.06	0.03–0.14
Maximum mercury injection/%	82.84	73.9–90.33	77.56	57.6–90.26	77.94	63.53–95.57	70.04	56.16–83.29
Mercury ejection efficiency/%	28.54	23.4–39.5	24.31	15.2–34.71	26	15.36–37.43	20.19	14.44–32.17
Sample amount/piece	4		9		12		6	

monitoring and automatic data acquisition and output results by the computer system are shown in Figs. 10, 11 and 12.

Casting thin section and scanning electron microscope observations

By injecting stained liquid glue into the pore space under vacuum pressure, casting thin sections are made after the consolidation of the liquid glue. In this study, Leica DMRXHC and Linkam THMSG600 optical microscopy instruments at the State Key Laboratory of Continental Dynamics of Northwest University, China are used to observe thin sections with the thickness of 0.03 mm and the area of no less than 15 mm × 15 mm. A total of 98 pieces of casting thin sections are observed under the polarizing microscope. American-manufactured FEI Quanta 650FEG device at the State Key Laboratory of Continental Dynamics of Northwestern University, China is used for scanning electron microscope analysis, which utilizes electron beam to scan the surface of 62 core samples. Scanning electron microscopy observation can help analyze the morphology of pores, throats, and clay minerals so as to reflect changes in the microscopic characteristics of rocks (Fig. 4).

Results and discussions

Microscopic pore structure characteristics

Petrological characteristics and reservoir space types

According to the petrological analysis, the main type of sandstone in Chang 6_3 reservoir of Huaqing oilfield is lithic feldspar sandstone, followed by feldspar sandstone and feldspar lithic sandstone (Fig. 3). The average contents of quartz, feldspar, and lithic fragment in the study area are, respectively, 28.01, 36.62, and 19.58%. The lithic fragment is dominated by metamorphic one, with few igneous and sedimentary ones. The porosity ranges between 5.22 and 3.43%, with an average of 8.78%, while the permeability varies from 0.003 to 0.63×10^{-3} μm^2, with an average of 0.22×10^{-3} μm^2. Therefore, it can be safely concluded that these are low porosity and ultra-low permeability reservoirs.

According to scanning electron microscope and casting thin section analyses, the main pore types in the Chang 6_3 reservoir are residual intergranular pores (Fig. 4a) and the feldspar solution pores (Fig. 4b). In addition, there are a few micro fractures (Fig. 4f), which can better connect the separated pores and thus greatly improve the reservoir permeability and connectivity. The primary pore combinations in the study area are intergranular pore–dissolution pore and dissolution pore–intergranular pore, among

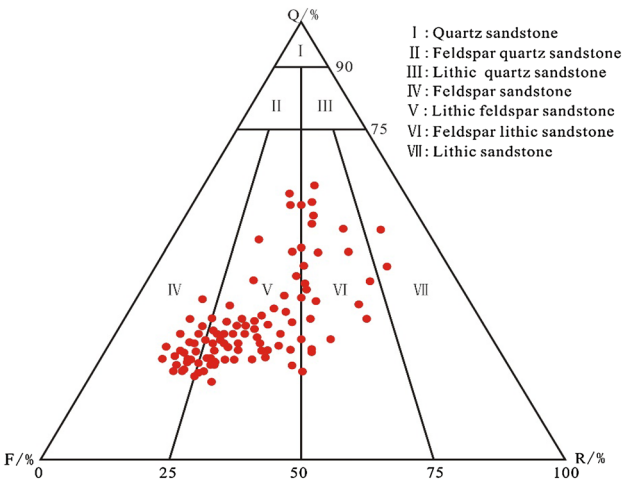

Fig. 3 Chang 6_3 reservoir sandstone classification scheme

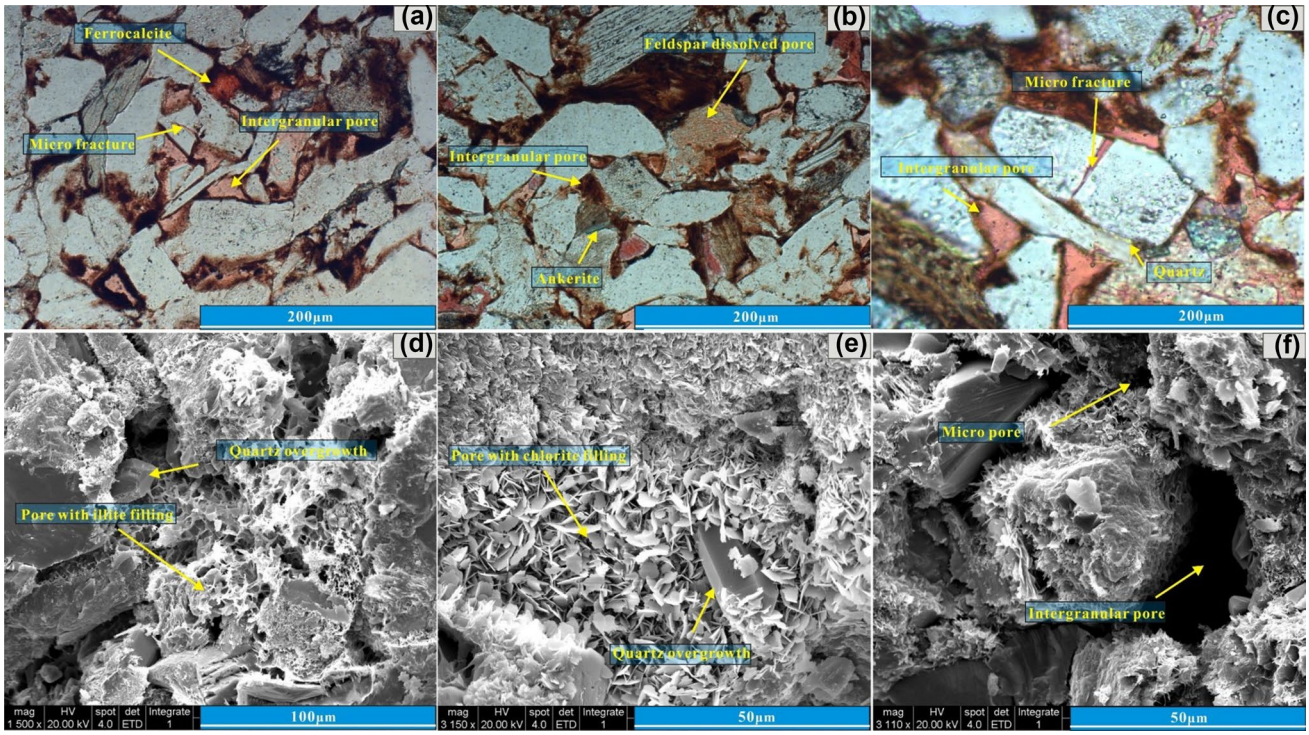

Fig. 4 Photos of casting thin sections and scanning electron microscope of Chang 6_3 reservoir in Huaqing oilfield. **a** Residual intergranular pores, well L87, 2195.45 m, Chang 6, casting thin section; **b** some feldspar dissolution pores, Well S156, 2071.45 m, Chang 6, casting thin section; **c** micro pores, Well W61, 2014.9 m, Chang 6, scanning electron microscope; **d** chlorite filling pores and throats, Well Y414, 1999.15 m, Chang 6, scanning electron microscope; **e** filiform illite filling pores and throats, Well B181, 2187.3 m, Chang 6, scanning electron microscopy; **f** micro fractures, Well B259, 2191 m, Chang 6, plane-polarized light, casting thin section

which the former type is more common. There are also a few micro pores (Fig. 4c). Dissolution effect in the diagenetic process alters the reservoir properties, resulting in larger pores and increased permeability and porosity (Fig. 4). Clay minerals are mainly illite and chlorite (Fig. 4d–e). Kaolinite is rarely developed. Ferrocalcite and ankerite are the main carbonates. Throats are in the forms of disc, curved disc and bundle. The reservoir is of overall poor connectivity and low throat coordination number. The pore structure distribution characteristics and the materials filled between the pores directly affect the reservoir storage and seepage capacities.

Pore structure types and features

According to the results of high-pressure mercury injection experiments on 31 cores, this study classifies the pore structures into four types based on analysis of the capillary pressure curve characteristics, displacement pressure, and mercury injection during different pressure intervals, namely types I, II, III and IV (Table 2; Fig. 5).

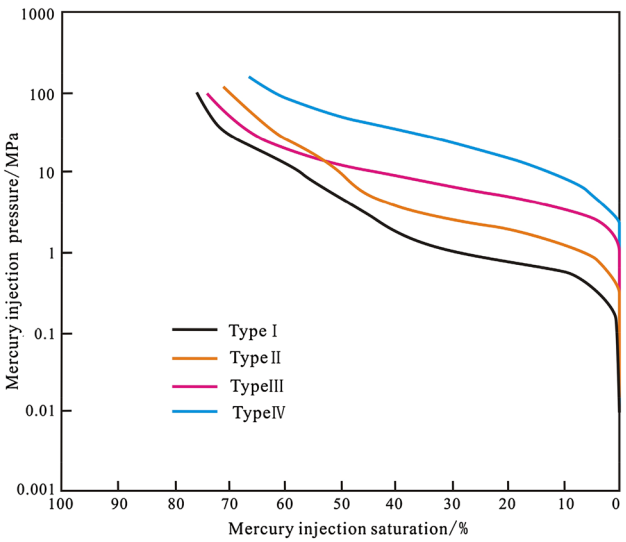

Fig. 5 Capillary pressure curves corresponding to different types of pore structures in Chang 6_3 reservoir in Huaqing oilfield

1. Type I pore structure featured by low displacement pressure, coarse skewness, good sorting, and high maximum mercury injection

The shape of the capillary pressure curve of type I pore structure is skewed towards the lower left of the figure, in which low displacement pressure means large permeability, coarse pore and throat radius, and good sorting. The displacement pressure ranges between 0.46 and 1.07 Mpa, with an average of 0.80 Mpa; the sorting coefficient ranges between 1.32 and 2.53, with an average of 1.90; the permeability ranges between 0.31 and 0.63×10^{-3} μm^2, with an average of 0.43×10^{-3} μm^2; and the average maximum mercury saturation is 82.84%. All these indicate excellent reservoir and seepage capacity, and the corresponding reservoirs are generally distributed in the thickest sandstone body in the underwater distributary channels.

2. Type II pore structure featured by low–medium displacement pressure, coarse skewness, medium–good sorting, and medium–high maximum mercury injection

The shape of the capillary pressure curve of type II pore structure is also skewed towards the lower left of the figure, but such pore structure has higher displacement pressure than the Type I pore structure, and it is also featured by high permeability, coarse pore and throat radius, and medium–good sorting. The displacement pressure ranges between 0.72 and 2.31 Mpa, with an average of 1.44 Mpa; the sorting coefficient ranges between 0.8 and 2.46, with an average of 1.63; the permeability ranges between 0.18 and 0.29×10^{-3} μm^2, with an average of 0.23×10^{-3} μm^2; and the average maximum mercury saturation is 77.56%. All these indicate good reservoir and seepage capacity, and the corresponding reservoirs are generally distributed in the underwater distributary channels or the side part proximal to the channel streamline.

3. Type III pore structure featured by high displacement pressure, fine skewness, medium sorting, and medium maximum mercury injection

The shape of the capillary pressure curve of type III pore structure is skewed towards the upper right of the figure, which indicates high displacement pressure, small permeability, good sorting, and fine pore and throat radius. Generally, high displacement pressure corresponds to poor reservoir capacity. The displacement pressure ranges between 1.49 and 3.22 Mpa, with an average of 2.3 Mpa; the sorting coefficient ranges between 0.79 and 2.61, with an average of 1.34; the permeability ranges between 0.09 and 0.21×10^{-3} μm^2, with an average of 0.14×10^{-3}μm^2; and the average maximum mercury saturation is 77.94%. All these indicate moderate reservoir and seepage capacity, and the corresponding reservoirs are generally distributed in the side part of underwater distributary channels or the side part proximal to the channel streamline.

4. Type IV pore structure featured by high displacement pressure, very fine to fine skewness, poor sorting, and small maximum mercury injection

The shape of the capillary pressure curve of type IV pore structure is more skewed towards the upper right of the figure, and there is rarely a flat interval in the range below SH-50. The displacement pressure ranges between 1.91 and 3.79 Mpa, with an average of 2.84 Mpa; the sorting coefficient ranges between 0.52 and 1.99, with an average of 1.07; the permeability ranges between 0.003 and 0.05×10^{-3} μm^2, with an average of 0.03×10^{-3} μm^2; and the average maximum mercury saturation is 70.04%. The corresponding reservoirs of type IV pore structure are the poorest in terms of reservoir and seepage capacity, and they are generally distributed in the side part of inter-distributary bay or the sandstone–mudstone interbedding (Fig. 6).

Microscopic water flooding characteristics in reservoirs with different pore structures

1. Type I pore structure

There are three pieces of cores with type I pore structure, with the average porosity of 10.50%, average permeability 0.47×10^{-3} μm^2, average throat radius 1.28 μm, average pore throat radius ratio 156.78, and average water-free stage displacement efficiency 22% (Table 3). Observation under microscope indicates homogeneous and reticular-homogeneous displacement (Fig. 8a–b). The water preferentially flows through the low resistance direction, with some breakthrough in the fracture direction. After the water breakthrough, the sweeping area is gradually expanded until covering the whole area with some oil film and corner residual oil (Fig. 8f–g). The water-free stage in the water flooding process of type I pore structure is relatively short, but the ultimate oil displacement efficiency is still relatively high, with the ultimate-stage displacement efficiency range of 37.1–42% (averaging 39.03%). Among all the four types of pore structures, type I pore structure is of the highest ultimate-stage displacement efficiency (Zhao et al. 2011).

2. Type II pore structure

There are also three pieces of cores with Type II pore structure, with the average porosity of 9.50%, average permeability 0.28×10^{-3} μm^2, average throat radius 0.563 μm, average pore throat radius ratio 395.013, and average water-free stage displacement efficiency 14.63% (Table 3). Generally, compared to type I pore structure, type II pore structure is featured by better physical properties, more effective pores and throats, but poorer pore throat radius distribution.

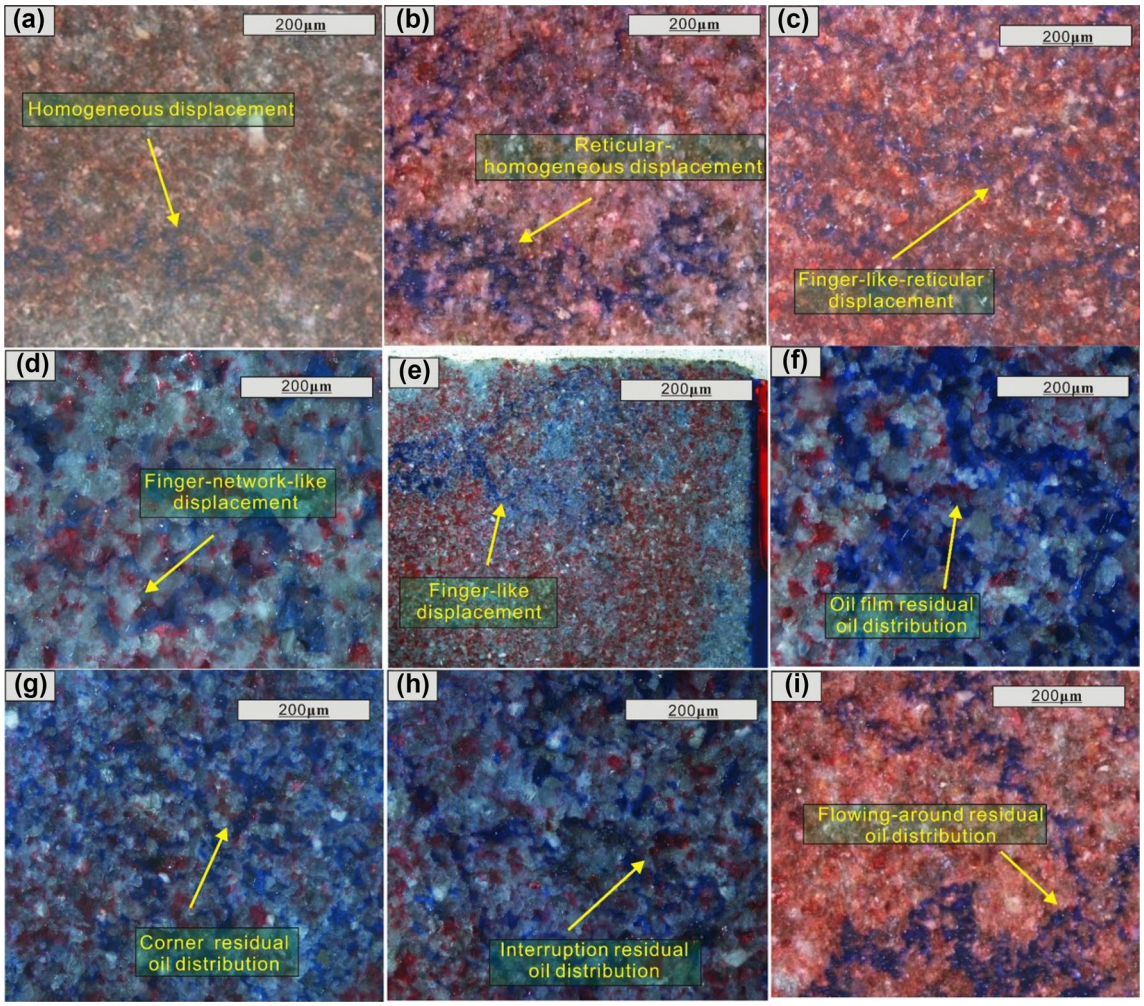

Fig. 6 Water flooding characteristics in reservoirs with different pore structures in Chang 6_3 reservoir in Huaqing oilfield. **a** Homogeneous displacement, Well L87, 2195.45 m; **b** reticular-homogeneous displacement, Well B461, 1985.71 m; **c** finger-like-reticular displacement, Well S156, 2071.45 m; **d** finger-network-like displacement, Well X245, 1976.8 m; **e** finger-like displacement, Well W71, 1948.57 m; **f** oil film residual oil distribution, Well W38, 2043.35 m; **g** corner residual oil distribution, Well B461, 1985.71 m; **h** interrupted residual oil distribution, Well S156, 2071.45 m; **i** flowing-around residual oil distribution, Well X245, 1976.8 m

Observation under microscope indicates dominant reticular-homogeneous displacement with a few finger-like-reticular displacement (Fig. 8b–d). Oil remaining in the reservoir is mainly the oil film residual oil and the flowing-around residual oil (Fig. 8f, i). After the breakthrough of reticular water flooding front, the sweeping area gradually increases, and the dominant displacement is reticular-homogeneous. The ultimate-stage displacement efficiency varies from 33.9 to 35% with an average of 34.47%, which is the secondary high among four types of pore structures.

3. Type III pore structure

There are also three pieces of cores with type III pore structure, with the average porosity of 7.79%, average permeability 0.14×10^{-3} μm^2, average throat radius 0.323 μm, average pore throat radius ratio 576.59, and average water-free stage displacement efficiency 14.13% (Table 3). Compared to type II pore structure, type III pore structure is featured by poorer physical properties, less effective pores and throats, and obviously poorer pore throat radius distribution. Observation under microscope indicates dominant finger-like-reticular displacement with a few finger-like displacement, and oil remaining in the reservoir is mainly the flowing-around residual oil (Fig. 8i). The ultimate-stage displacement efficiency varies from 29.7 to 36% with an average of 32.03%, which is the secondary low among four types of pore structures.

4. Type IV pore structure

Table 3 Water flooding results of microscopic real sandstone model of Chang 6_3 reservoir in Huaqing oilfield

Pore structure type	Well	Porosity/%	Permeability/$10^{-3}\mu m^2$	Original oil saturation/%	Water-free stage			Ultimate stage		
					Displacement efficiency/%		Main displacement way	Displacement efficiency/%		Main displacement way
					Single sample	Mean		Single sample	Mean	
I	W38	13.43	0.69	64.6	25	22	Homogeneous	42	39.03	Homogeneous
	L87	8.70	0.31	57.7	19.4		Reticular-homogeneous	37.1		Homogeneous
	B461	9.38	0.40	59	21.6		Reticular-homogeneous	38		Reticular-homogeneous
II	S156	9.03	0.41	52.6	13.9	14.63	Reticular-homogeneous	33.9	34.47	Reticular-homogeneous
	B168	8.93	0.20	53.8	14.4		Finger-like-reticular	34.5		Reticular-homogeneous
	B259	10.53	0.22	55.4	15.6		Finger-like-reticular	35		Reticular-homogeneous
III	W61	6.79	0.05	49.1	15	14.13	Finger-like-reticular	29.7	32.03	Finger-like-reticular
	X245	6.18	0.10	50	10.4		Finger-like-reticular	30.4		Finger-like-reticular
	Y414	10.41	0.27	56	17		Finger-like-reticular	36		Finger-like-reticular
IV	B181	7.82	0.09	51.5	12.6	11.75	Finger-like	32.4	29.75	Finger-like-reticular
	W71	5.22	0.08	58.8	10.9		Finger-like	27.1		Finger-like

There are also three pieces of cores with type IV pore structure, with the average porosity of 6.52%, average permeability 0.086×10^{-3} μm^2, average throat radius 0.495 μm, average pore throat radius ratio 416.904, and average water-free stage displacement efficiency 11.75% (Table 3). Type IV pore structure is of the poorest physical properties, strongest effective pore throat heterogeneity, and poorest pore throat radius distribution. Observation under microscope indicates dominant finger-like displacement (Fig. 8e), and oil remaining in the reservoir is mainly interrupted and flowing-around residual oil (Fig. 8h–i). The ultimate-stage displacement efficiency is 29.75%, which is the lowest among four types of pore structures.

Factors affecting water flooding efficiency

The exploration and development practices and theories of Yanchang and Yan'an Formations in the Ordos Basin demonstrate the reservoir heterogeneity to be an important factor affecting the microscopic water flooding of sandstones, and the microscopic pore structure to be the key factor hindering the development of low and ultra-low permeability reservoirs. The microscopic pore structure of reservoirs can directly and objectively reflect the development benefits of reservoirs. Accordingly, possible factors influencing oil displacement efficiency are analyzed in the following part, including porosity, permeability, reservoir quality, throat radius, pore throat radius ratio, sorting coefficient, and movable fluid saturation.

Physical properties

Physical property experiments indicate the poor physical properties of Chang 6_3 reservoir in Huaqing oilfield. The water-free and ultimate stage oil displacement efficiencies are both positively correlated with porosity, with respective correlation coefficients of 0.4185 and 0.7216 (Fig. 7), while they are more positively correlated with permeability, with respective correlation coefficients of 0.6365 and 0.8008 (Fig. 8). The relative strong relationship between the permeability and oil displacement efficiency as well as the higher correlation coefficient between it and ultimate stage oil displacement efficiency indicates the stronger permeability of effective throat network, which contributes to the more seepage paths with wider range and larger sweeping area and finally larger ultimate stage oil displacement efficiency. The reservoir quality index, which is a function of permeability and porosity, is more strongly correlated with water-free and ultimate stage oil displacement efficiencies, with respective correlation coefficients of 0.6879 and 0.8829 (Fig. 9), which suggests that single physical parameter cannot faithfully reflect the seepage properties. The displacement efficiency

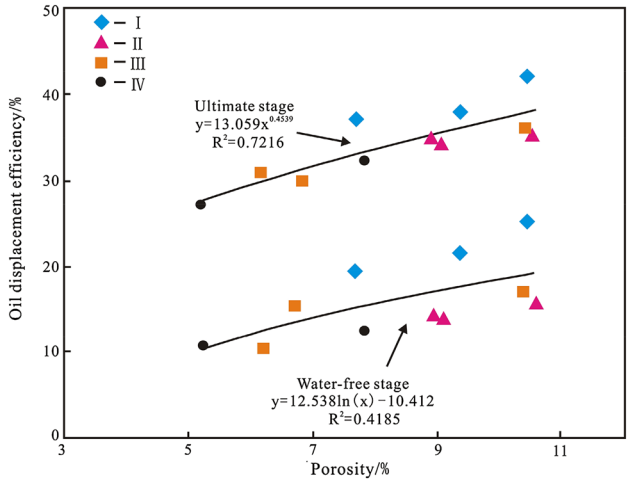

Fig. 7 Relationship between reservoir porosity and oil displacement efficiency

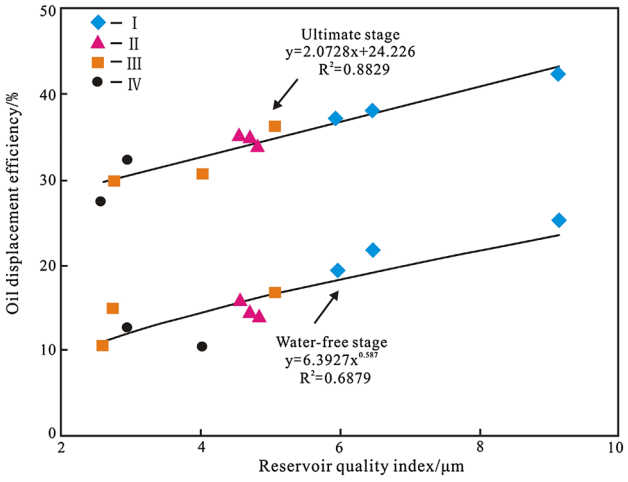

Fig. 9 Relationship between reservoir quality index and oil displacement efficiency

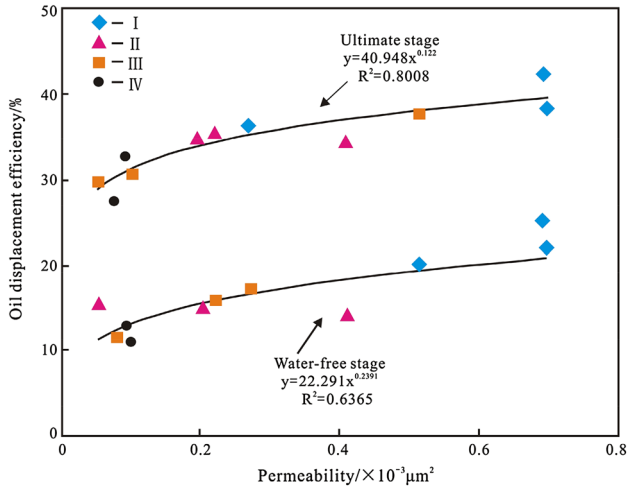

Fig. 8 Relationship between reservoir permeability and oil displacement efficiency

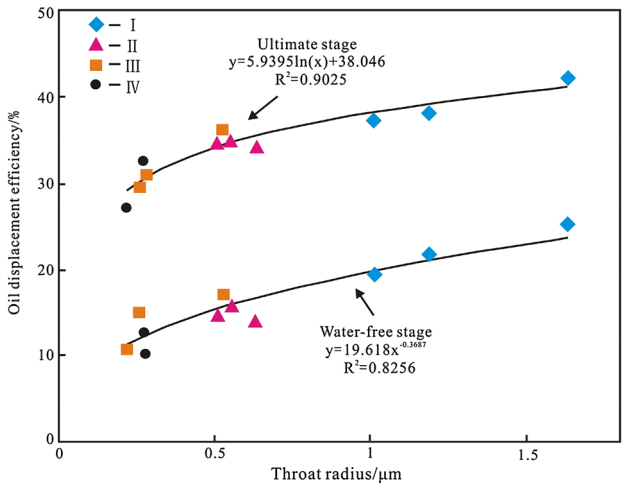

Fig. 10 Relationship between throat radius and oil displacement efficiency

is not completely controlled by single reservoir parameters, and it has certain independence.

Microscopic pore structure

1. Throat radius

The average pore throat radius is positively correlated with the water-free and ultimate stage oil displacement efficiencies, with respective correlation coefficients of 0.8256 and 0.9025 (Fig. 10). When the throat radius is less than 1 μm, oil displacement efficiency sharply increases with the increasing throat radius, which then turns to be gentle when the throat radius is greater than 1 μm. This indicates the influence of throat radius and throat permeability contribution curve on oil displacement efficiency. Under the same experimental conditions, more evenly distributed throat radius can contribute to smoother seepage path, larger sweeping area, and higher displacement efficiency when it comes to the throats with similar or equal radius. As the main factor influencing oil displacement efficiency, throat radius can more intuitively and truly characterize the reservoir under the action of sedimentary and diagenetic alternation.

2. Pore throat radius ratio

Figure 11 shows the relatively good negative correlation between the pore throat radius ratio and the water-free and ultimate stage oil displacement efficiencies, with respective correlation coefficients of 0.7772 and 0.8274. It can

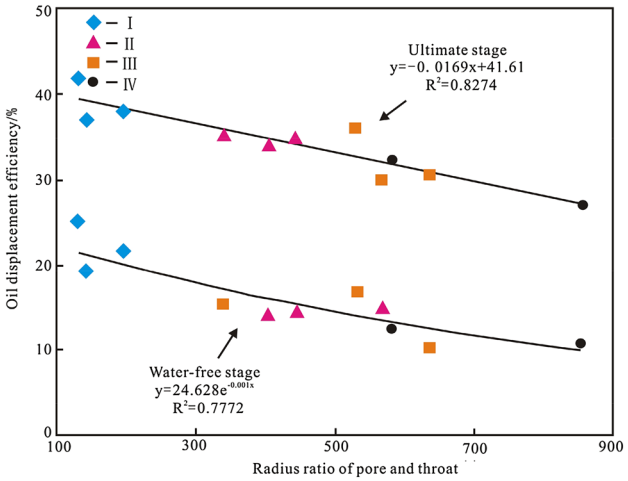

Fig. 11 Relationship between pore throat radius ratio and oil displacement efficiency

be indicated that larger pore throat radius ratio corresponds to poorer pore throat connectivity and larger displacement resistance. Under the same experimental conditions, the relatively high-permeability zone is featured by bypass flow, small sweeping area, and low oil displacement efficiency. Meanwhile, the smaller pore throat radius generally corresponds to closer size of pores and throats as well as more uniform distribution of them, which means smaller heterogeneity coefficient and thus higher seepage capacity and ultimate stage oil displacement efficiency.

3. Sorting coefficient

As can be seen from Fig. 12, the water-free and ultimate stage oil displacement efficiencies are positively correlated with the sorting coefficient, with respective correlation coefficients of 0.5747 and 0.853. Larger sorting coefficient means larger structural seepage coefficient, wider throat radius distribution, better pore structure in the low-permeability reservoir, more uniform pore and throat distribution, more macro throats, stronger flow capacity, and thus higher oil displacement efficiency under different displacement pressures.

Movable fluid saturation

Movable fluid saturation parameters are widely used in the research of reservoir seepage mechanism to evaluate the fluid seepage capacity in the reservoir. As shown in Fig. 13, the correlations between the movable fluid saturation and water-free and ultimate stage oil displacement efficiency are relatively good, with respective correlation coefficients of 0.803 and 0.8839. Such high correlation is comparable to the correlation between reservoir quality index and microscopic pore structure and oil displacement efficiency, and higher than that between porosity and permeability and oil displacement efficiency. Generally, larger movable fluid saturation corresponds to stronger seepage capacity of the reservoir, more seepage channels, larger sweeping area, and thus higher oil displacement efficiency under different displacement pressures.

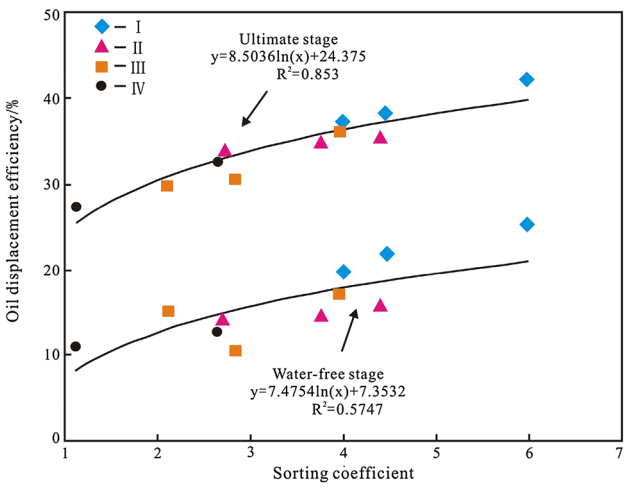

Fig. 12 Relationship between sorting coefficient and oil displacement efficiency

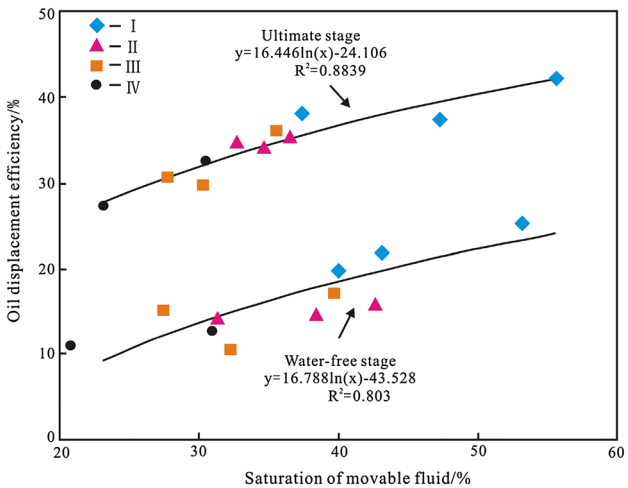

Fig. 13 Relationship between movable fluid saturation and oil displacement efficiency

Conclusions

The Chang 6_3 reservoir in Huaqing oilfield, Ordos Basin, China is classified as the low porosity and ultra-low permeability reservoir, with the average porosity of 8.77% and the average permeability of 0.22×10^{-3} μm^2. There is a very close relationship between microscopic pore structure characteristics and water flooding efficiency. Through the microscopic real sandstone model water flooding experiments of 11 core samples and other microscopic experiments, this study comprehensively investigates the fluid flow law in the rock pore space. Consequently, the following conclusions are drawn:

1. The Chang 6_3 reservoir in Huaqing oilfield is a set of tight sandstone reservoir, with the main effective lithology of gray and gray-brown lithic feldspathic sandstone and feldspar sandstone, followed by a small amount of feldspar lithic sandstone. The primary interstitial materials are illite and chlorite, and kaolinite is rarely developed. Residual intergranular pores are the dominant pore types, followed by some feldspar dissolution pores. The sorting is moderate, and the intergranular pore–feldspar dissolution pore combination takes the majority.
2. According to the capillary pressure curve characteristics and comprehensive analysis of corresponding parameters, the pore structure of Chang 6_3 reservoir is divided into four types, namely types I–IV, with corresponding worsening reservoir and seepage capacities. Type II and III pore structures mostly develop in the study area. Observed displacement patterns are reticular-homogeneous as well as finger-like-reticular, with the oil displacement efficiency decreasing.
3. There are obvious differences in the water displacement pattern and oil displacement efficiency among four types of pore structures. The size and distribution of the throat radius are the key factors affecting the water flooding efficiency; better reservoir properties contribute to higher oil displacement efficiency; better pore structure corresponds to larger throat radius, better sorting, more macro pores and throats, more uniform pore throat distribution, and consequently higher oil displacement efficiency; the pore throat radius ratio is the most important parameter to characterize the reservoir heterogeneity, and the smaller pore throat radius ratio means closer size between pores and throats, resulting in the higher seepage capacity and ultimate stage oil displacement efficiency; microscopic pore structure parameters are key factors that affect oil displacement efficiency.

References

Bai R, Li Z, Wang H, Liu X, Wei Q, Li H (2016) Fractal nature of microscopic pore throat structure in Chang 7 tight oil reservoir of Longdong area. Sci Technol Eng 16(5):54–59

Cao L, Sun W, Sheng J, Huo L, Chen Q, Xie C (2016) A method to determine movable fluid saturation of low-permeability and tight oil reservoirs-by taking tight oil reservoirs in sixth member of Yanchang formation in Banqiao area as an example. J Yangtze Univ (Natural Science Edition) 13(20):1–8 (**in Chinese**)

Clarkson CR, Jensen JL, Pedersen PK, Freeman M (2012) Innovative methods for flow-unit and pore-structure analyses in a tight siltstone and shale gas reservoir. AAPG Bull 96:355–374

Dastgheib S, Amoozegar M, Elahi E, Asad S, Banat I (2008) Bioemulsifier production by a halothermophilic Bacillus strain with potential applications in microbially enhanced oil recovery. Biotechnol Letter 30(2):263–270

Dong H, Hong Y, Rui W (2006) The effect of wettability on oil recovery of alkaline/surfactant/polymer flooding, SPE 102564. In: Annual technical conference and exhibition, San Antonio, TX, USA, September 24–27

Gao H, Wang X, Qi Y (2013) Characteristics of NMR water displacing oil and influencing factors in extra-low permeable sandstones: taking the yanchang group in Ordos Basin as an example. Geol J China Univ 19(2):59–63 (**in Chinese**)

Ge X, Fan Y, Li J, Zahid MA (2015) Pore structure characterization and classification using multifractal theory—an application in Santanghu Basin of western China. J Pet Sci Eng 127:297–304

Guo W, Hou Z, Shi M, Wu X (2007) The recovery mechanism and application of Brevibacillus brevis and *Bacillus cereus* in extra-low permeability reservoir of Daqing. Pet Exp Dev 01:73–78

Halim A, Nielsen S, Lantz A, Suicmez V, Lindeloff N, Shapiro A (2015) Investigation of spore forming bacterial flooding for enhanced oil recovery in a North Sea chalk reservoir. J Pet Sci Eng 133:444–454

Huang H, Ren D, Zhou Y, Sun W, Liu D (2016) Characteristics of movable fluid and pore evolution of the Chang 8_1 sandstone reservoirs of the Ordos Basin. J Northwest Univ (Natural Science Edition) 46(5):735–745 (in Chinese)

Jia C (2017) Breakthrough and significance of conventional oil and gas to classical petroleum geology theory. Pet Exp Dev 44:1–10

Kamath VA, Yang J, Sharma GD, 1993. Effect of asphaltene deposition on dynamic displacements of oil by water. SPE 26046-MS. In: Presented at SPE Western Regional Meeting, Anchorage, Alaska, May 26–28

Kaster K, Hiorth A, Eilertsen G, Boccadoro K, Lohne A, Berland H, Stavland A, Brakstad O (2012) Mechanisms involved in microbially enhanced oil recovery. Transp Porous Med 91:59–79

Kate JM, Gokhale CS (2006) A simple method to estimate complete pore size distribution of rocks. Eng Geol 84:48–69

Lappin-Scott H, Cusack F, Costerton J (1988) Nutrient resuscitation and growth of starved cells in sandstone cores: a novel approach to enhanced oil recovery. Appl Environ Microbiol 6:1373–1382

Li S, Guo P, Du J, Wang Y (2007) New way to improve gas well production and condensate gas field's recovery factor. J Southwest Pet Univ (Nat Sci Ed) 29:1–6

Liu Z, Yue X, Hou J, Zhang L (2002) Comparison of displacement oil mechanism of polymer, ASP and foam of ASP in micro pores and dead-ends of pores. In: SPE 77876, Asia Pacific oil and gas conference and exhibition, Melbourne, Australia, October 8–10

Ma X, Gao H, Zhang J, Xue Q (2016) Optimization of determination method for dehydrogenase activity of crude enzyme preparation from fungi. J Northwest A&F Univ (Nat Sci Ed) 44:55–161

Papadimitriou NI, Romanos GE, Charalambopoulou GCh, Kainourgiakis ME, Katsaros FK, Stubos AK (2007) Experimental investigation of asphaltene deposition mechanism during oil flow in core samples. SPE J 57(3):281–293

Qin J, Zhang K, Chen X (2010) Mechanism of the CO_2 flooding as reservoirs containing high water. Acta Pet Sin 31(5):797–800

Qu X, Sun W, Lei Q, Huang H, Huo L (2016) Study on saturation of movable fluid in the low-permeability sandstone reservoirs of Huaqing oilfield and its influencing factors. J Northwest Univ (Natural Science Edition) 31(2):93–98 (in Chinese)

Rabiei A, Sharifinik M, Niazi A, Hashemi A, Ayatollahi S (2013) Core flooding tests to investigate the effects of IFT reduction and wettability alteration on oil recovery during MEOR process in an Iranian oil reservoir. Appl Microbiol Biot 13:5979–5991

Ren X, Li A, Wang Y, Wu S, Wang G (2015a) Pore structure of tight sand reservoir and its influence on percolation-taking the Chang 8 reservoir in Maling oilfield in Ordos Basin as an example. Oil Gas Geol 36(5):774–779. in Chinese

Ren D, Sun W, Zhao J, Qu X, Zhang X (2015b) Microscopic waterflooding characteristics of lithologic reservoirs in Ordos Basin and its influence factors: taking the Chang 8_1 reservoir in Huaqing oilfield as an example. J China Univ Min Technol 44(6):1043–1052 (**in Chinese**)

Shi J, Qu X, Lei Q, Fu B, He Y, Zhao G, Cheng L (2016) Distribution characteristics and controlling factors of movable fluid in tight oil reservoir: a case study of Chang 7 reservoir in Ordos Basin. Nat Gas Geosci 27(5):827–834 (**in Chinese**)

Song Z, Zhu W, Sun G, Blanckaert K (2015) Dynamic investigation of nutrient consumption and injection strategy in microbial enhanced oil recovery (MEOR) by means of large-scale experiments. Appl Microbiol Biotechnol 15:6551–6561

Suthar H, Hingurao K, Desai A,. Nerurkar A (2008) Evaluation of bioemulsifier mediated microbial enhanced oil recovery using sand pack column. J Microbiol Methods 75:225–230

Wang X, Gu Y (2011) Oil recovery and permeability reduction of a tight sandstone reservoir in immiscible and miscible CO_2 flooding processes. Ind Eng Chem Res 50(4):2388–2399

Wang R, Chen J, Sun W (2008) Application of CT image technique to the research of oil displacement with water drive in ultra-low permeability sandstone reservoir. Prog Geophys 23:864–870 (**in Chinese**)

Wardlaw NC (1982) The effects of geometry, wettability, viscosity and interfacial tension on trapping in single pore-throat pairs. J Can Pet Technol 82:21–27

Xia W, Luo Z, Dong H, Yu L (2013) Studies of biosurfactant for microbial enhanced oil recovery by using bacteria isolated from the formation water of a petroleum reservoir. Pet Sci Technol 21:2311–2317

Yadali JB, Kharrat R (2009) Fundamental study of pore morphology effect in low tension polymer flooding or polymer-assisted dilute surfactant flooding. Transp Porous Med 76:199–218

Yadali JB, Kharrat R (2010) Analysis of microscopic displacement mechanisms of dilute surfactant flooding in oil-wet and water-wet porous media. Transp Porous Med 81:1–19

Yan J, Liang Q, Geng B, Lai F, Weng D, Wang Z (2017) Relationship between micro-pore characteristics and pore structure of low permeability sandstone: a case of the fourth member of Shahejie Formation in southern slope of Dongying Sag. Lithol Reserv 29(3):18–26 (**in Chinese**)

Yang P, Guo H, Yang D (2013) Determination of residue oil saturation during waterflooding in tight oil formations with NMR relaxometry measurements. Energy Fuels 27(10):5750–5756

Zanganeh P, Ayatollahi S, Alamdari A, Zolghadr A, Dashti H, Kord S (2012) Asphaltene deposition during CO_2 injection and pressure depletion: a visual study. Energy Fuel 26(2):1412–1419

Zhang X, Xu D, Zhu C, Lundaa T, Scherr KE (2012a) Isolation and identification of biosurfactant producing and crude oil degrading *Pseudomonas aeruginosa* strains. Chem Eng J 41:138–146

Zhang J, Wang P, Xue Q, Lai H, Zhao J (2012b) Isolation of bacteria for MEOR in the Yanchang oilfield and their biodegradation characteristics. J Northwest A&F Univ (Nat Sci Ed) 40:118–128

Zhang X, Ren D, Ren Q, Huang H, Liu D, Qu X (2015a) Microscopic waterflooding characteristics of lithologic reservoirs in Ordos Basin and its influence factors: taking the Chang 8_1 reservoir in Huaqing oilfield as an example. J China Univ Min Technol 45(2):284–290 (**in Chinese**)

Zhang Y, Pe-Piper G, Piper DJ (2015b) How sandstone porosity and permeability vary with diagenetic minerals in the Scotian Basin, offshore eastern Canada: implications for reservoir quality. Mar Pet Geol 63:28–45

Zhang J, Xue Q, Gao H, Xin M, Ping W (2016) Biodegradation of crude oil by fungal enzyme preparations from *Aspergillus* spp. for potential use in enhanced oil recovery. J Chem Technol Biotechnol 91:865–875

Zhao YC, Song YC, Liu Y, Liang HF, Dou BL (2011) Visualization and measurement of CO_2 flooding in porous media using MRI. Ind Eng Chem Res 50(8):4707–4715

Zhao L, Ma T, Gao M, Gao P, Cao M, Zhu X, Li G (2012) Characterization of microbial diversity and community in water flooding oil reservoirs in China. World J Microbiol Biotechnol 28:3039–3052

Zhao X, Dang H, Pang Z, Shi P, Cao S, Ding L, Bai P (2017) Microscopic pore structure and seepage characteristics of different pore assemblage types in ultra low permeability reservoir: a case of Chang 6 reservoir in Tang 157 well area, Ganguyi oilfield. Lithol Reserv 29(6):9–14 (**in Chinese**)

Zheng Q, Liu Y (2015) Microscopic pore structure and movable fluid saturation of ultra low permeability reservoir. Geol Sci Technol Inf 34(4):124–131 (**in Chinese**)

Zhou Y, Ji Y, Xu L, Che S, Niu X, Wan L, Zhou Y, Li Z, You Y (2016) Controls on reservoir heterogeneity of tight sand oil reservoirs in Upper Triassic Yanchang Formation in Longdong Area, southwest Ordos Basin, China: implications for reservoir quality prediction and oil accumulation. Mar Pet Geol 78:110–135